Geophysical Journal (1989) **97**, 511–527

Topography and geoid undulations caused by small-scale convection beneath continental lithosphere of variable elastic thickness

Gabriele Marquart* and Harro Schmeling†

* *University of Uppsala, Institute of Geophysics, Department of Geodesy, Hällby, S-75590 Uppsala, and † University of Uppsala, Institute of Geology, Department of Mineralogy and Petrology, Box 555, S-75122 Uppsala, Sweden*

Accepted 1988 November 29. Received 1988 November 28; in original form 1987 August 24

SUMMARY

The effect of subcontinental upper mantle convection on topography, gravity and geoid undulation is studied with special regard to the effective elastic thickness of the continental lithosphere (h_{el}). We designed a numerical model of the upper mantle–lithosphere system consisting of a constant viscosity fluid overlayed by a partly elastic plate. The boundary tractions (stresses) at the top of the convecting mantle model were applied to the lithosphere model for which we used the thin plate approximation. The total thickness of the lithosphere was kept constant to 150 km while the elastic thickness was varied between 0 and 150 km. The aspect ratio of the convecting mantle was varied between 0.7 and 3 and the Rayleigh number between 10^4 and 10^6. Our calculations demonstrate the effect of a thick elastic lithosphere on the surface observables: peak to peak averaged amplitude of topography, geoid undulation and gravity are strongly reduced and their spectra are low pass filtered. For an aspect ratio less than 1 and a very thick elastic lithosphere topography tends to zero and while geoid undulation and gravity may even become negative above the upwelling plume. The spectral relation of geoid or gravity to topography (admittance) is nearly unaffected for $h_{el} < 70$ km. For $h_{el} > 70$ km admittance values for all wavelengths generally decrease with increasing elastic thickness of the plate and may become negative. Geoid admittance for the basic mode increases with larger aspect ratio, while gravity admittance for $h_{el} < 100$ km slightly decreases. Associating higher Rayleigh numbers of the convecting fluid with lower viscosity, an increase in Rayleigh number leads to considerable decrease of the surface observables. However, admittance values are only slightly affected and decrease approximately linearly with increasing Rayleigh number. Comparison of our results with observations of the topography spectrum and the free air gravity admittance for North America suggests that large aspect ratio cells beneath continents are unlikely. However, convection cells of aspect ratio 1 or less underlying an elastic lithosphere of at least 100 km thickness is in agreement with data. The Rayleigh number should be as high as 10^6.

Key words: sublithospheric convection, continental lithosphere, elastic plate bending, topography, geoid, gravity, admittance

1 INTRODUCTION

1.1 Sublithospheric convection

Even though the existence of convection in the earth's mantle is generally accepted, the pattern of the flow is highly debated. While the velocity pattern of the plates directly represent the surface expression of large-scale mantle convection, evidence for small-scale convection beneath the plates can be obtained only indirectly. Theoretical and experimental investigations demonstrate the possibility of three dimensional convection cells or longitudinal rolls, parallel or orthogonal to the velocity of oceanic plates (see, e.g. Richter 1973; Richter & Parsons 1975; Schmeling 1987). Interpretations of gravity and geoid anomalies suggest the existence of such convective rolls or cells beneath the Pacific and Indic plates (McKenzie *et al.* 1980; Haxby & Weissel 1986).

What are the indications for convection beneath continents? Convective flows beneath a lithosphere may be associated with variations in lithospheric thickness. A convecting sublithospheric mantle would lead to perturbations of the temperature field within the lithosphere/asthenosphere system deflecting the isotherms upwards (downwards) above up-welling (down-welling) regions. Due to the strong temperature dependence of the rheology the base of the (mechanical or thermal) lithosphere may be defined by the depth of a particular isotherm. Thus lateral variations of the lithospheric thickness may at least partly reflect the dynamics of a convecting mantle below. Without a dynamic mantle, temperature variations at the base of the

lithosphere would equilibrate after a characteristic time of a few hundred Ma. Maps of the lithospheric thickness (e.g. Babuska, Plomerora & Sileny 1987, for a seismological lithosphere) indicate significant variations of the thickness with typical wavelengths of about 1000 km corresponding roughly to aspect ratio 1 upper mantle convection.

Another indication for sublithospheric convection results from heat flow data. Sclater, Jaupart & Galson (1980) attributed small-scale convection beneath continents to be the mechanism controlling the steady state thermal structure of continental lithosphere. Estimates of the reduced heat flow (i.e. the heat flow entering the base of the crust) from different continental regions show lateral variations between 15 and 90 mW m^{-2} (Vitorello & Pollack 1980) or 15–30 mW m^{-2} if regions with Cenozoic tectonic activity are excluded (Pujol, Fountain & Anderson 1985). Such variations are typical for convection; however, the latter variations may also be partly due to the different cooling times of the different regions. Intraplate volcanism and continental rifting processes strongly require convective mantle flows beneath at least some continental regions.

Sublithospheric convective flows may play an important role during aggregation and dispersal of continents as demonstrated by numerical models of Gurnis (1988). In the models of Schmeling & Jacoby (1981) and Christensen (1983) it was shown that a subducting oceanic plate may induce subcontinental convection rolls.

1.2 Geoid, gravity, topography and the elastic lithosphere

To test the possibility of subcontinental convection we will use surface observables such as topography, geoid undulations, and gravity. In contrast to oceanic plates the elasticity of a thick continental plate will play a major role in the relation between these observables and mantle convection, and therefore will receive special attention.

Thermally driven flow in the mantle transfers stresses to the base of the lithosphere resulting in deformation of the surface, i.e. topography. Thermal density contrasts in the mantle and lateral density disturbances due to deflected interfaces or the surface lead to geoid undulations and gravity anomalies. In the following the spectral ratio of geoid to topography will be named geoid admittance and the spectral ratio of gravity to topography gravity admittance. Admittance values have been calculated for a number of different convection problems, focussing on temperature dependent viscosity, boundary conditions, two-layer convection, and sphericity and self-gravitation of the earth (McKenzie 1977; Parsons & Daly 1983; Ricard, Fleitout & Froidevaux 1984; Richards & Hager 1984; Cserepes & Rabinowicz 1985; Koch & Yuen 1985).

McKenzie (1977) studied upper mantle convection in a constant viscosity fluid and showed that for the wavelength range 2000–3000 km both the gravity and topography show a positive anomaly over the upwelling flow, indicating that the dominant effect arises from the surface deflection. However, some authors (e.g. Hager 1984; Koch & Yuen 1985; Ritzert, personal communication) found that the surface observables highly depend on the viscosity structure: negative topography may occur over upwelling regions if the viscosity increases strongly with depth. Richards & Hager (1984) calculated potential and surface deformation Love numbers for a variety of internal density contrasts. These density contrasts were treated as load functions and regarded as results of different types of mantle convection and vicosity stratification in a spherical earth. They found a negative correlation between topography and geoid only for spherical harmonics of degree and order less than 9 and viscosity contrasts beween upper and lower mantle of about 2 orders of magnitude. It should be noted, that in the case of constant viscosity, positive admittance is found for all wavelengths for one layer convection.

A global study of the relationship between observed geoid (*SEASAT*) and topography (Cazenave *et al.* 1986; Cazenave & Dominh 1987) for the wavelength range 1000–4000 km showed positive correlation for all wavelengths with values around 2.5–5 m km^{-1}. Generally their values are low compared to results from theoretical studies by Parsons & Daly (1983) who obtained admittance values of about 6–8 m km^{-1} for a broad range of wavelengths.

Most calculations of mantle flow treated only the case of convection beneath oceanic plates, whereby the thin oceanic lithosphere was not taken into account. Some studies, however, focussed on subcontinental convection (e.g. Fleitout & Yuen 1984), but modelled the lithosphere as a highly viscous non-elastic sheet. However, for the convecting earth buoyancy forces leading to topography and thus geoid undulations may be partly compensated by elastic stresses within the lithosphere. While for long wavelengths elastic compensation is negligible, it will be important for wavelengths shorter than a transitional wavelength λ_t (e.g. Turcotte & Schubert 1982). λ_t depends on the elastic thickness of the lithosphere and can be estimated by bending theory of a thin elastic plate overlying a viscous fluid:

$$\lambda_t = 2\pi\left(\frac{g\cdot\rho_0}{D}\right)^{-1/4}. \tag{1a}$$

Here g is the gravity acceleration and ρ_0 is the density of the sublithospheric mantle. Inserting the definition of the flexural rigidity D of the lithosphere in (1a)

$$D = \frac{E\cdot h_{el}^3}{12(1-\nu^2)}$$

gives the dependence of the transitional wavelength from the elastic thickness of the lithosphere

$$\lambda_t = 2\pi\left(\frac{12(1-\nu^2)}{E} g\rho_0 h_{el}^{-3}\right)^{-1/4}, \tag{1b}$$

where E is Young's modulus, ν is the Poisson ratio and h_{el} is the effective elastic thickness. h_{el} characterizes that part of the lithosphere in which bending stresses do not relax during times comparable to the characteristic time of loading. Inspecting equation (1b) indicates that for oceanic lithosphere ($h_{el} < 50$ km) elastic compensation of bending is negligible for wavelengths larger than 1000 km. This was also found by McKenzie & Bowin (1976), Watts & Daly (1981) and Watts & Ribe (1984). However, the elastic thickness increases with age by cooling of the plate (Watts, Bodini & Ribe 1980) and plays an important role during subduction. For continental lithosphere the effective elastic thickness might be greater, affecting topographic and geoid

undulations for wavelengths even larger than 500 km (*cf.* equation 1).

The behaviour of a loaded elastic plate is dependent on the wavelength of the load. Thus the geoid and gravity admittances are also sensitive to the elastic thickness of the lithosphere. Increasing the elasticity of the plate (or decreasing the wavelength of the load) will decrease the topographic contribution of the geoid or gravity, thereby decreasing the admittances, in the extreme case down to negative values.

In our approach we will systematically study the influence of a lithosphere with variable elastic thickness on topography, geoid and gravity. For simplicity we restrict ourselves to constant viscosity in the mantle and assume a number of convective rolls extending between the base of the lithosphere and 670 km depth.

2 THE CONTINENTAL LITHOSPHERE

The thickness of the continental lithosphere can be estimated from a number of different geophysical observations. However, the different time-scales and nature of the geophysical processes involved require different definitions of the lithosphere. Interpretation of heat flux data (Sclater *et al.* 1980; Davies & Strebeck 1982) gave a thermal lithospheric thickness of 150–200 km, defined by the depth to the 1200 °C geotherm (e.g. Pollack & Chapman 1977). The uncertainty in thickness is mainly due to the unknown amount of radiogenic heating in the lower crust and uppermost mantle.

Seismological studies on body wave travel times and Rayleigh wave dispersion (Souriau & Souriau 1983) indicated a very thick seismological continental lithosphere of at least 200 km.

Walcott (1970) determined the thickness of the mechanical lithosphere from its flexural rigidity as a response of surface ice load. He obtained values of about 120 km. Wolf (1987) studied postglacial adjustment of the Fennoscandian lithosphere using a three layer Maxwell half-space for the Earth. He obtained 80 km of lithospheric thickness.

Peltier & Wu (1983) estimated the mechanical continental lithosphere to be 260 km thick by studying polar wander induced by deglaciation. Yuen, Sabadini & Boschi (1983) studied the rotational polar wander in a dynamic earth and estimated the global averaged mechanical lithospheric thickness to 150–200 km. These results suggest that the thickness of the mechanical continental lithosphere will be of the order of 120–200 km for loading times of the order of 10^4 yr.

On larger time-scales elastic thicknesses somewhat less than the mechanical thicknesses mentioned above were found by Karner & Watts (1983), who studied the gravity anomalies and flexure of the lithosphere at three different mountain ranges and got values between 50 to 130 km. However, for the Alps elastic thickness as low as 25 km might also be possible.

Kogan & McNutt (1987) studied the state of isostasy in the USSR by calculating admittance due to Bouguer gravity anomalies. For that part of the old shield bearing the Ural, they found values for the flexural rigidity D of about 10^{24} Nm which corresponds to about 100 km elastic lithosphere.

Forsyth (1985) modelled the observed transfer function between gravity and topography for the Kenya rift valley with an elastic plate approach. He found a rather low value for the flexural rigidity favouring an effective elastic thickness of the plate of about 30 km. However, this value is taken from a tectonic active region with a presumably thinned lithosphere. For old, stable continental shields or platforms it can be expected that the effective elastic thickness will be higher.

A clue to a better understanding of lithospheric structure on different time scales are rheological strength profiles. The strength of the material is strongly dependent on temperature. Possible temperature gradients for continental lithosphere can be obtained from textbooks (e.g. Turcotte & Schubert 1982). Molnar & Tapponnier (1981) calculated a number of reasonable continental geotherms by varying crustal heat generation, thermal conductivity and heat flux at the lithosphere base. According to their results we assumed two possible geotherms for old stable continental areas which are given in Fig. 1. The heat flux at the base of the lithosphere in 150 km depth was about 20 mW m^{-1} which corresponds to a temperature of around 1300 °C. For steady-state creep of many materials at moderate stresses ($<10^2$ MPa) the creep strength ($\sigma_1 - \sigma_3$) is related to the strain rate $\dot{\varepsilon}$ and the temperature T by

$$\sigma_1 - \sigma_3 = \left(\frac{\dot{\varepsilon}}{A^*}\right)^{1/n} \exp\left(\frac{Q^* - V^*P}{nR^*T}\right), \qquad (3)$$

where R^* (gas constant) is 8.31 J (mol K)$^{-1}$, and A^*, n, the activation energy Q^* and the activation volume V^* can be determined from experiments (Weertman 1970; Stocker & Ashby 1973; Goetze 1978). P is the pressure.

To estimate the lithospheric strength it has been suggested (Goetze & Evans 1979) that the continental crust is

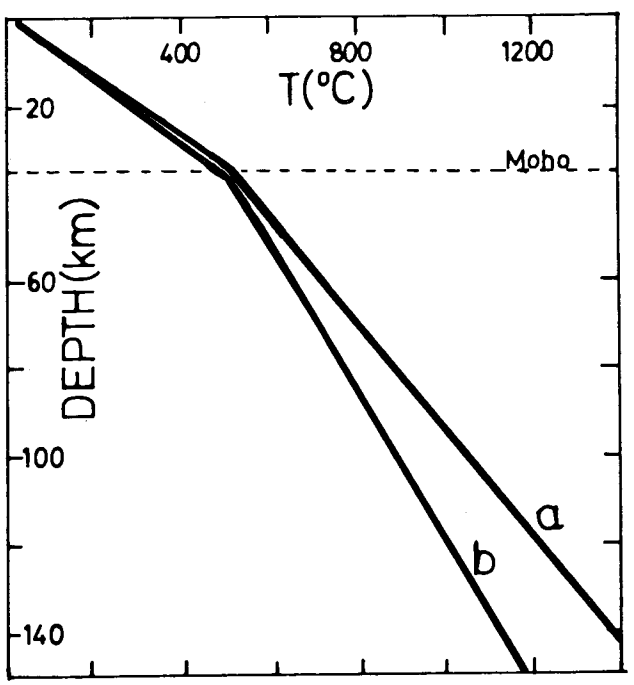

Figure 1. Simplified geotherms for old stable continental lithosphere. Heat flux at lithosphere base about 20 mW m^{-2}, at the surface above 50 mW m^{-2}.

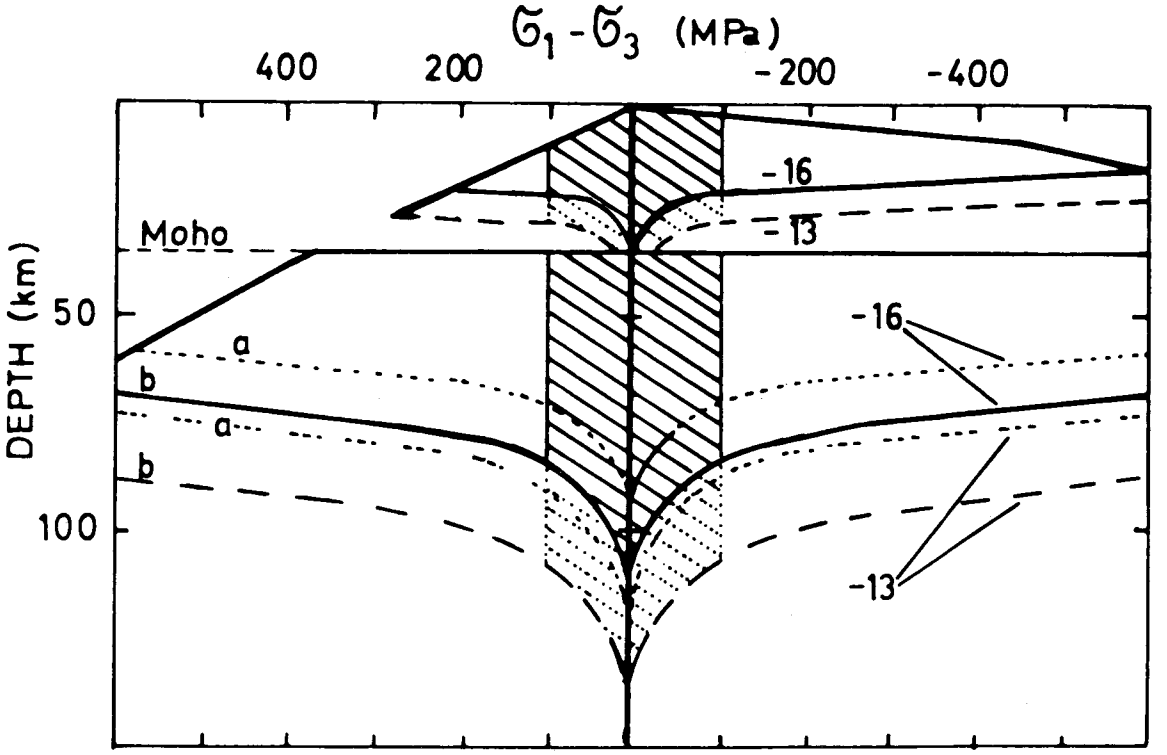

Figure 2. Strength profiles for continental lithosphere assuming geotherms a and b from Fig. 1. The frictional coefficient was 0.5. The numbers besides the curves give $\log_{10} \dot{e}$. The shaded area indicates the elastic lithosphere as seen by convection.

controlled by quartz rheology while olivine rheology represents the mantle. Olivine is generally accepted as the major rock-forming mineral in the mantle and its rheological parameters are summarized by Goetze (1978). However, the uncertainty in creep strength for olivine is still on the order of 1 magnitude. For quartz the material parameters are even less well known and it is obviously a rough approximation to model the strength of the crust only by quartz. The material constants for a large number of quartz minerals are summarized by Kirby (1983).

In the uppermost crust the strength is governed by frictional sliding on faults (Byerlee 1978). We assumed a frictional coefficient of 0.5, the geotherms from Fig. 1 and the following material parameters for the creep law given in equation (3).

Quartz: $\log A^* = -2.48[\mathrm{MPa}^{-n}\,\mathrm{s}^{-1}]; n = 3;$
$Q^* = 2.0 \times 10^5\,\mathrm{J\,mol}^{-1}$

Olivine: $\log A^* = 4.84[\mathrm{MPa}^{-n}\,\mathrm{s}^{-1}]; n = 3;$
$Q^* = 5.23 \times 10\,\mathrm{J\,mol}^{-1}.$

The activation volume V^* was not considered because of its minor influence on lithospheric behaviour. These parameters lead to strength profiles given in Fig. 2. In our calculations it turned out that sublithospheric small-scale convection produces lithospheric stresses as small as 10–100 MPa. Typical strain rates for materials taking part in convective flow are on the order of 10^{-13} to $10^{-14}\,\mathrm{s}^{-1}$. The strain rates leading to bending of the lithosphere due to changing convection patterns are of the order of $10^{-16}\,\mathrm{s}^{-1}$ or less. If we accept these numbers, inspection of Fig. 2 leads to the conclusion that the elastic thickness of the old stable continental lithosphere will be of the order of 80–100 km. The region between the different strain rate curves represents that part of the lithosphere which yields viscously during bending on the time-scale of 10^9 yr but which is so high in viscosity that it effectively does not take part in convective circulation.

3 THE MODEL

To understand how a partly elastic continental lithosphere deforms due to mantle convection, we divided the lithosphere–upper mantle system into a plate model and a viscous convecting mantle model which were mechanically coupled (Fig. 3). In the mantle model convection was assumed to occur in the form of two-dimensional steady-state rolls between the lithospheric base and the 670 km interface. The viscosity was taken constant. No thermal interaction between asthenosphere and lithosphere was taken into account. The mechanical coupling was approached by assuming a no-slip boundary condition (i.e. zero velocity) at the upper boundary of the convection model and by taking the surface tractions (i.e. stress vectors) of the convective flow as a load function for the plate model. This gives us the advantage to model a free surface to determine the topography. The variable input parameters of the model are the aspect ratio (a) and the Rayleigh number (Ra) and the thickness of the elastic part of the lithosphere. The aspect ratio varied between 0.7 and 3; this corresponds to lateral cell dimensions between 364 and 1560 km. Values between 2.4×10^4 and 2.4×10^6 were assigned to the Rayleigh number (see definition below). For the elastic thickness we choose values between 0 and 150 km, but kept the entire thickness of the lithosphere constant at 150 km in

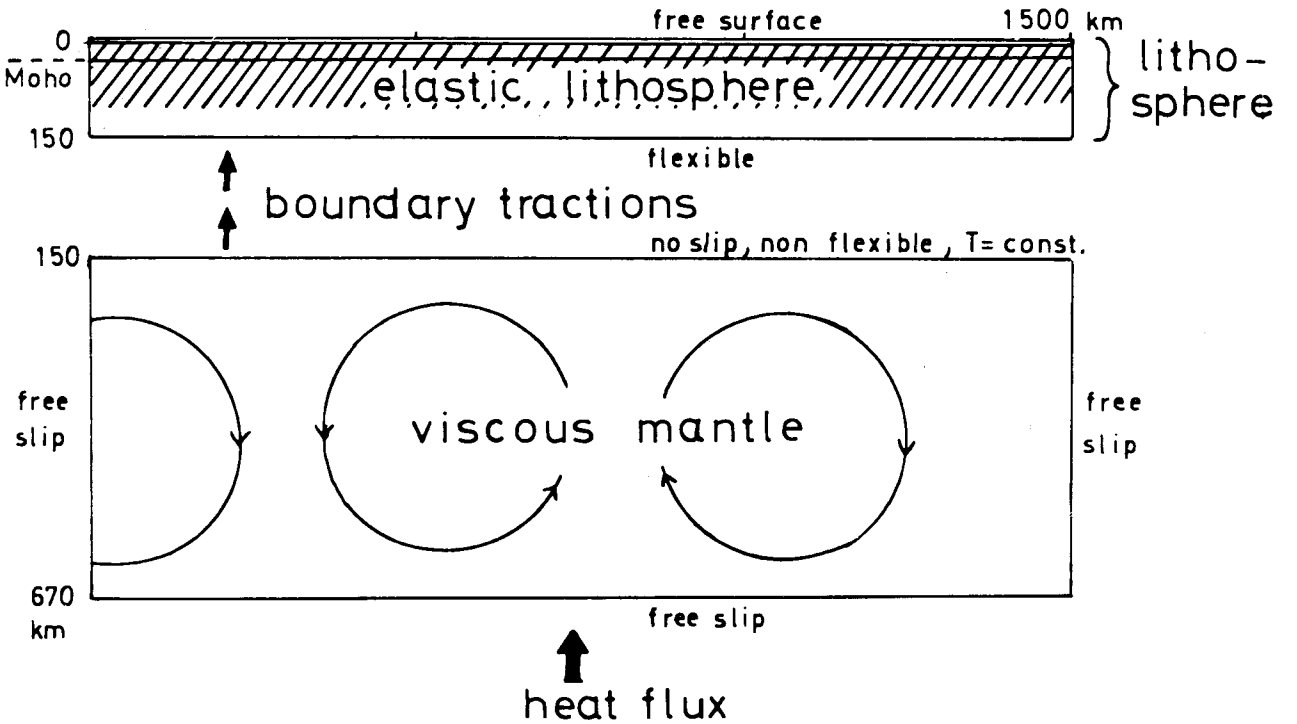

Figure 3. Schematic diagram of our model. The lithosphere is not thermally coupled to the convection mantle, but dynamically by the upper boundary tractions of the convecting model.

most of the models. However, for some of the models the thickness of the lithosphere itself was varied.

The output parameters of the models are the surface topography, the gravity and the geoid undulations. From these we calculated the geoid admittance A and the gravity admittance R. Both functions are a criterion to decide if spectral components of geoid or gravity are dominated by the convecting mantle or the deflection of the lithosphere.

3.1 Mathematical approach

Thermal convection in the earth can be described by the equations of mass, momentum, energy conservation and by the equation of state. Following basically Jarvis & McKenzie (1980) the equations for steady state flow of a compressible fluid (anelastic liquid approximation) of infinite Prandtl number and a constant viscosity reduce to a non-dimensional form (primes indicate non-dimensional variables)

$$2\frac{\partial^2}{\partial x'\,\partial z'}\left[e^{z'(Di/\Gamma)}\left(2\frac{\partial^2\psi'}{\partial x'\,\partial z'}+\frac{Di}{\Gamma}\frac{\partial\psi'}{\partial x'}\right)\right]+\left(\frac{\partial^2}{\partial z'^2}-\frac{\partial^2}{\partial x'^2}\right)\left[e^{z'(Di/\Gamma)}\left(\frac{\partial\psi'^2}{\partial z'^2}-\frac{\partial\psi'^2}{\partial x'^2}+\frac{Di}{\Gamma}\frac{\partial\psi'}{\partial z'}\right)\right]=Ra\,\rho_r'\frac{\partial T'}{\partial x'}-\frac{Di}{\Gamma}\frac{\partial P'}{\partial x'} \tag{4}$$

$$\rho_r'\mathbf{u}'\nabla T'-Di\,\rho_r'(T'+T_0')u_z'=\nabla^2T'+\phi', \tag{5}$$

where ψ' is the stream function, Di the dissipation number, Γ the Grüneisen parameter (both assumed constant), Ra the Rayleigh number which is only a scaling parameter here, $\rho_r'(z)$ the reference density profile according to the Adams Williamson equation, P' the non-hydrostatic pressure, T_0' the absolute temperature at the top of the convective layer, T' the temperature above T_0', ϕ' the energy dissipation, $\mathbf{u}'$ the velocity field and u_z' the vertical component of it. The non-dimensional quantities ρ_r', Ra and Di are given as

$$\rho_r'=e^{(1-z')(Di/\Gamma)} \tag{6a}$$

$$Ra=\frac{\rho_m g\alpha\,\Delta T\,d^3}{\kappa\eta} \tag{6b}$$

$$Di=\frac{dg\alpha}{c_p}. \tag{6c}$$

For definitions of the parameters in (6), see Table 1.

These equations are solved in a rectangular box with a no-slip boundary condition at the top and a free-slip boundary condition at the sides and bottom (Fig. 3). As

Table 1. Values for upper mantle parameters used in this study.

ρ_m:	reference density	$3400\ \mathrm{kg\,m^{-3}}$
g:	gravity acceleration	$9.81\ \mathrm{m\,s^{-2}}$
α:	thermal expansivity	$3.7\times10^{-5}\ \mathrm{K^{-1}}$
ΔT_1:	scaling temperature	1000 °C
T_0:	temperature at the top of the convecting layer	1300 °C
q:	bottom heat flux	$20\ \mathrm{mW\,m^{-2}}$
d:	thickness of convecting mantle	$5.2\times10^5\ \mathrm{m}$
k:	thermal conductivity	$4.42\ \mathrm{W\,m^{-1}\,K}$
c_p:	specific heat at constant pressure	$1.3\times10^3\ \mathrm{J\,kg^{-1}\,K}$
κ:	thermal diffusivity	$10^{-6}\ \mathrm{m^2\,s^{-1}}$
η:	viscosity	$1.7\times10^{21}\ \mathrm{Pa\,s}$
Γ:	Grüneisen parameter	1.1

temperature boundary conditions we assumed constant temperature at the top, no heat flow across the sides and a constant heat flow at the bottom. The side boundaries are reflective, implying a periodic continuation of the flow pattern. With the bottom heat flux q, a physical Rayleigh number can be defined (McKenzie, Roberts & Weiss 1974)

$$Ra_q = \frac{g\alpha q\, d^4}{c_p \kappa^2 \eta}. \tag{7}$$

As stated before, Ra (or Ra_q) was a variable input parameter. However, Table 1 summarizes a set of values typical for the earth which lead to a medium Rayleigh number of $Ra = 102\,000$ or $Ra_q = 240\,000$.

Equations (4) and (5) are solved by a finite difference method described by Schmeling (1980) and Schmeling & Jacoby (1981) which has been extended to include compressibility.

To calculate the load function for the lithospheric plate on top of the convecting mantle it is necessary to determine the tractions at the upper surface of the convecting part of the model. Because of the no-slip boundary condition both normal and shear tractions occur.

The normal tractions σ_{z0} and the shear tractions σ_{x0} at the top of the convection model are given as the components of the stress vector p_i (the summation convection is assumed)

$$p_i = \sigma_{ij}\hat{n}_j|_{\text{top}} = \left(\frac{\sigma_{xz}}{\sigma_{zz}}\right)_{\text{top}} \equiv \left(\frac{\sigma_{x0}}{\sigma_{z0}}\right), \tag{8}$$

where $\hat{n}_j$ is the surface normal vector and σ_{ij} is the stress tensor

$$\sigma_{ij} = -P\,\delta_{ij} + \eta\left(\frac{\partial u_i}{\partial x_j} + \frac{\partial u_j}{\partial x_i}\right). \tag{9}$$

Here δ_{ij} is the Kronecker delta, P is the fluid pressure and u_i is the flow velocity vector.

The deflection of the lithosphere depends on both vertical and horizontal tractions. σ_{x0} transmits a bending moment to the plate resulting in deflection with opposite sign of that due to σ_{z0}. This leads to a reduction of the whole topography. For a further discussion of the effect of σ_{x0}, see below.

While the velocities can be directly obtained by taking the derivatives of the streamfunction, the pressure has to be determined by numerical integration of the compressible Navier–Stokes equation. Since this procedure involves integration of third derivatives of the streamfunction, the resulting pressure has been checked carefully.

Tests with refined grids (up to 81×61) and integrations along different paths showed that the pressure inside the box is accurate with an integration error less than 0.2 per cent. Deviations between different integration paths are maximum near the corners of the box, but are less than 4 per cent in all cases shown. While such localized inaccuracies are transmitted to topography and geoid directly in case of zero lithospheric thickness, they are damped out for finite thicknesses.

For the lower boundary the normal tractions $(\sigma_{zz})_{\text{bottom}} \equiv \sigma_{z1}$ can be determined similarly. Since at the 670 km interface no forces can be sustained elastically, σ_{z1} will be completely balanced by the deflection of the interface, w_{MB} (McKenzie 1977). With $\Delta\rho_{\text{MB}}$ as the density jump at that interface we have

$$w_{\text{MB}}(x) = \frac{1}{g\,\Delta\rho_{\text{MB}}} \cdot \sigma_{z1}. \tag{10}$$

However, in the case of additional lower mantle convection one has to use $\Delta\sigma_{z1}$ instead of σ_{z1}, $\Delta\sigma_{z1}$ being the difference between upper and lower mantle normal stresses at the boundary. Then $\Delta\sigma_{z1}$ depends on the type of coupling between upper and lower mantle convection.

3.2 Calculation of surface topography

To determine the surface topography of a partly elastic lithosphere overlying a number of small-scale convection cells we mainly used the thin elastic plate approximation. The governing differential equation is

$$D\frac{d^4w}{dx^4} + \rho_0 g w = p(x), \tag{11}$$

where w is the deflection taken as positive in upwards direction, $p(x)$ the load function and ρ_0 the density of the underlying material. In our case the load function is represented by the normal tractions due to convection. These functions are periodic and symmetric with respect to $x = 0$ due to the periodicity of the model. Therefore σ_{z0} (equation 8) can be expanded into a Fourier series

$$\sigma_{z0} = \sum_{n=1}^{\infty} \sigma_{z0_n} \cos(nkx); \qquad k = 2\pi/\lambda_1. \tag{12}$$

λ_1 is the wavelength of the basic mode which is twice the horizontal dimension of the investigated model. We found the solution of equation (11) for a periodic load function to be

$$w(x) = -\sum_{n=1}^{\infty} [\rho_0 g + D(nk)^4]^{-1} \cdot \sigma_{z0_n} \cos(nkx). \tag{13}$$

Due to the $1/h_{\text{el}}^3$ dependence of D, $w(x)$ is also very sensitive to the elastic thickness h_{el} of the plate and an increase in h_{el} strongly decreases the surface topography. If the elastic thickness is assumed to be zero, which corresponds to purely isostatic, or better, 'isodynamic' adjustment, equation (13) reduces to

$$w_{\text{iso}}(x) = -\sum_{n=1}^{\infty} \frac{\sigma_{z0_n}}{\rho_0 g} \cos(nkx), \tag{14}$$

which is identical with the formula given by McKenzie (1977).

The thin-plate approximation as given in equation (11) describes the state of deformation of a plate if only normal forces are present and if the wavelength λ_1 of the load function is large compared to thickness of the plate. For a periodic load function all major spectral components have to be large compared to h_{el}.

Marquart (1987) has tested the validity of the thin plate approximation by comparing it to results from finite element calculations. She found good agreement between the two methods for $\lambda_1/h_{\text{el}} \geq 10$; for $\lambda_1/h_{\text{el}} \approx 5$ the deviation in deflection reaches about 20 per cent. The thin-plate approximation underestimates the real deflection due to its

inability to deform horizontally, therefore the plate appears stiffer.

On the other hand by using the thin-plate approximation we neglect the effect of horizontal tractions which tend to lower the amplitude of the deflection. If horizontal and vertical tractions are of the same order of magnitude, horizontal traction will lower the deflections by about 10 per cent for long wavelengths loading and by about 60 per cent for $\lambda_1/h_{el} \approx 5$. However, in the convection models the amplitude of horizontal tractions never reach more than half the value for the vertical one. For some of our convection models we calculated the deflection of the lithosphere by applying the finite element method using nodal forces calculated from the vertical and the horizontal tractions and compared the result of the thin-plate approximation. The results coincide within a few percent, even if $\lambda_1/h_{el} \approx 5$ due to the counteracting effects of assuming a thick plate and accounting for horizontal tractions.

3.3 Calculation of geoid undulations

For the determination of the geoid we followed a procedure outlined by Davies (1986). The basic assumption is that all density variations are represented by a number of mass sheets denoted by i at different depths z_{0i}. The density variation associated with a deflected boundary at depth z_{0i} can be approximated by a mass sheet with a mass density θ per unit area.

$$\theta(x, z_{0i}) = \Delta\rho_i w_i(x), \tag{15}$$

where $\Delta\rho_i$ is the difference between the density above and below the boundary i. Density variations $\Delta\rho(x, z)$ resulting from temperature and pressure variations can be obtained from the equation of state

$$\rho(x, z) = \rho_r(z)[1 - \alpha(T - T_s) + \beta(z)P)]. \tag{16}$$

Here T_s is the adiabatic reference temperature and β is the compressibility which is depth-dependent in the same way as ρ_r (a consequence of assuming Γ = constant). The density variations in thin horizontal layers of thickness δ_i are approximated by mass sheets at depth z_{0i}, $i = l_0, \ldots, l$. The thickness δ_i should be sufficiently small for vertical temperature variations to be neglected. The mass density distribution of one of these sheets at depth z_{0i} is

$$\theta_i(x) = \theta(x, z_{0i}) = \Delta\rho(x, z_{0i})\delta_i = [-\alpha(T(x, z_{0i}) - T_s) + \beta(z_{0i}) \cdot P(x, z_{0i})] \cdot \rho_r(z_{0i})\,\delta_i. \tag{17}$$

If we express $\theta_i(x)$ in a Fourier series with the Fourier coefficients θ_{ni}, the geoid undulations $N_i(x)$ due to a particular mass sheet i are given by (Davies 1986)

$$N_i(x) = \frac{2\pi G}{gk} \sum_{n=1}^{\infty} n^{-1}\theta_{ni} e^{-nkz_{0i}} \cos(nkx). \tag{18}$$

Here G is the gravitational constant.

The entire geoid anomaly due to l layers at different depths z_{0i} is given by

$$N(x) = \sum_{i=1}^{l} N_i(x). \tag{19}$$

For the lithosphere we assume three layers ($l = 3$) associated with density jumps $\Delta\rho_i$ at the surface, the Moho, and the lithospheric base. If the thin-plate theory is applicable, the deflection $w(x)$ inside the lithosphere is independent of z. In this case it follows from equations (13), (15) and (19) for the geoid undulation due to the deflection of a partly elastic lithosphere

$$N_L(x) = -\frac{2\pi G}{gk} \sum_{n=1}^{\infty} n^{-1}(\rho_m g + Dn^4k^4)^{-1} \times \sigma_{z0_n} \cos(nkx) \cdot \sum_{i=1}^{3} \Delta\rho_i e^{-nkz_{0i}}. \tag{20}$$

The geoid undulations due to density variations within the convecting region can be obtained by inserting the Fourier coefficients of θ_i for all mass sheets within the mantle (equation 17) into (19) (P_{ni}, ΔT_{ni} are the Fourier coefficients of P and $(T - T_s)$ of the ith sheet, respectively)

$$N_{TP}(x) = \frac{2\pi G}{gk}\rho_m \sum_{n=1}^{\infty} n^{-1} \cos(nkx) \times \sum_{i=1}^{l} e^{-nkz_{0i}}\delta_i[\beta(z_{0i})P_{ni} - \alpha\,\Delta T_{ni}]. \tag{21}$$

In our study we calculated N_{TP} with 40–60 layers of constant thickness δ_i (= 13–8.6 km).

From equations (10), (15) and (18) one can easily deduce the geoid undulation due to deflection of the upper mantle base at depth z_{0M}

$$N_M(x) = \frac{2\pi G}{g^2k} \sum_{n=1}^{\infty} n^{-1}\,\delta_{z1_n} e^{-nkz_{0M}} \cos(nkx). \tag{22}$$

Here σ_{z1_n} are the Fourier coefficients of the normal traction σ_{z1}. The geoid of the whole model is then given by

$$N(x) = N_L(x) + N_{TP}(x) + N_M(x). \tag{23}$$

The various parameters used for the geoid calculation are compiled in Table 2.

The contribution to the geoid due to compressibility alone, N_P, is of the order of 5 per cent of the thermally induced geoid undulations, N_T. On the other hand, N_T and N_L are of similar order, but opposite sign. Consequently, N_P might become important with respect to the total geoid undulation. The same is true for N_M which sensitively depends on the type of convection in the lower mantle.

The geoid admittance A as a spectral function is calculated by

$$A(\lambda) = \tilde{N}(\lambda)/\tilde{w}(\lambda), \tag{24}$$

where $\tilde{N}(\lambda)$ and $\tilde{w}(\lambda)$ are the spectra of N and w.

Even though the admittance values do not give direct information on the type of source, it is one of the few surface observables. For continental regions, however, it is often more convenient to consider gravity rather than the geoid, which is difficult to measure over continents.

Table 2. Values used for calculation of geoid undulation.

E: Young's modulus	1.5×10^{11} Pa
ν: Poisson ratio	0.29
ρ_c: mean crustal density	2600 kg m^{-3}
ρ_s: mean sub-Moho density	3000 kg m^{-3}

Therefore we related our geoid undulations to free air gravity anomalies in the spectral domain by

$$\widetilde{\Delta g}_{FA}(\lambda) = \frac{2\pi}{\lambda} \tilde{N}(\lambda) \cdot g. \tag{25}$$

The gravity admittance R is defined similar to (24) by

$$R(\lambda) = \widetilde{\Delta g}_{FA}(\lambda)/\tilde{w}(\lambda). \tag{26}$$

4 RESULTS

For the numerical modelling we solved equations (4) and (5) on an equidistant grid of 41×41 up to 81×61 points depending on the aspect ratio and Rayleigh number. Related to nature our convection models had a depth of 520 km, overlayed by a lithosphere of 150 km thickness. The horizontal dimensions varied between 364 and 1560 km depending on the aspect ratio 0.7 to 3. Convective flow had been initiated by small initial temperature perturbations. The Rayleigh number Ra was varied between 10^4 and 10^6, to study the dependence of geoid undulation and topography on the intensity of the flow. It should be noted here that all models were forced into steady state by over-relaxation technique. In addition, for aspect ratio 3 and $Ra = 10^5$ we calculated a model allowing for time dependence. The flow did not come into a steady state but showed periodic behaviour as it would be expected for an aspect ratio of 3 (Christensen 1987). The oscillation amplitudes of geoid and topography depend on h_{el}; for $h_{el} = 100$ km the maximum values for geoid and topography oscillate between 27 and 32 m and 1100 and 1300 m, respectively.

Some general effects common in all models are shown in Fig. 4 for aspect ratio 1 and $Ra = 10^5$: the boundary tractions (Fig. 4a), the geoid undulation, its contributions and the surface topography for an effective elastic thickness of the lithosphere of 0 (Fig. 4b) and 150 km (Fig. 4c).

Although the top and bottom boundary conditions are not symmetrical, the ratio between top and bottom normal tractions, σ_{z0}/σ_{z1}, remains nearly constant and close to -1 for all models. However, the relation between the maximum shear to normal tractions, σ_{x0}/σ_{z0}, increases with decreasing aspect ratio: For $a = 3$ it is 0.13, for $a = 0.7$ the ratio increases to about 0.31.

Comparing Fig. 4(b) and (c) shows that a thick elastic lithosphere strongly decreases and smoothens the geoid undulations and topography. In particular, N_L is decreased while N_{TP} and N_M remain uneffected. Figure 5 shows the topography, total geoid undulation and geoid admittance as a function of the effective elastic thickness h_{el} again for aspect ratio 1. The full drawn lines in Fig. 5(a and b), indicate the peak to peak averaged amplitude in space domain for topography ($\tilde{w}$) and geoid ($\tilde{N}$) while the dashed lines give the values for the basic Fourier coefficients. The deviation between these curves are due to the low pass filter effect of the elastic plate. For $h_{el} < 50$ km higher order Fourier coefficients contribute significantly to the signal, for a thick plate only the fundamental mode is transmitted. Again, as seen in Fig. 4(b and c), topography and geoid are strongly reduced for increasing h_{el}.

We calculated the admittance for all our models. The

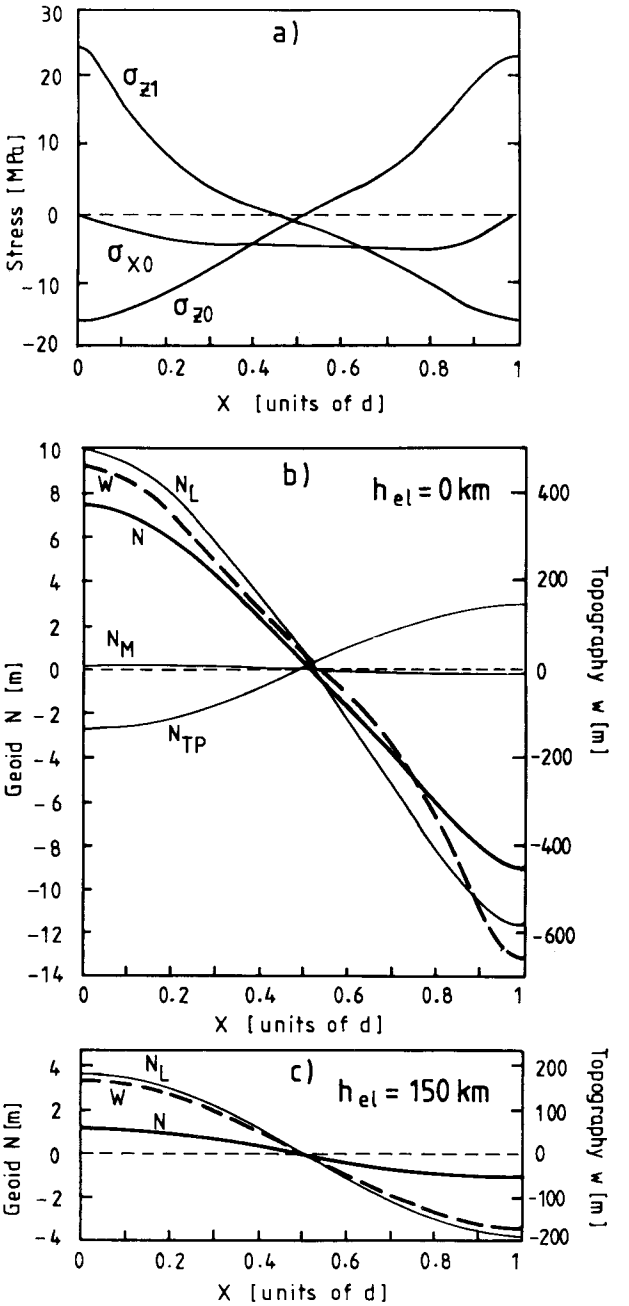

Figure 4. Results as functions of horizontal distance x for $a = 1$, $Ra = 10^5$. (a) σ_{z0} and σ_{x0}, vertical and horizontal tractions at lithosphere base; σ_{z1}, vertical tractions at 670 km depth. (b) Whole geoid undulation N, topography w and geoid contributions (N_{TP} thermal and pressure induced geoid, N_M geoid due to deflection of upper mantle base, N_L geoid due to deflection of lithosphere) for lithosphere with no flexural rigidity, $h_{el} = 0$ km. (c) Same as in (b) but for elastic bending throughout the lithosphere ($h_{el} = 150$ km). N_M and N_{TP} remain unchanged.

general behaviour is illustrated in Fig. 5(c) for $a = 1$ and $Ra = 10^5$. The admittance for the fundamental wavelength and overtones decreases (i) with increasing elastic thickness and (ii) with decreasing aspect ratio, indicating the increasing contribution of the thermal geoid of the mantle (see below). This leads to negative admittances for the

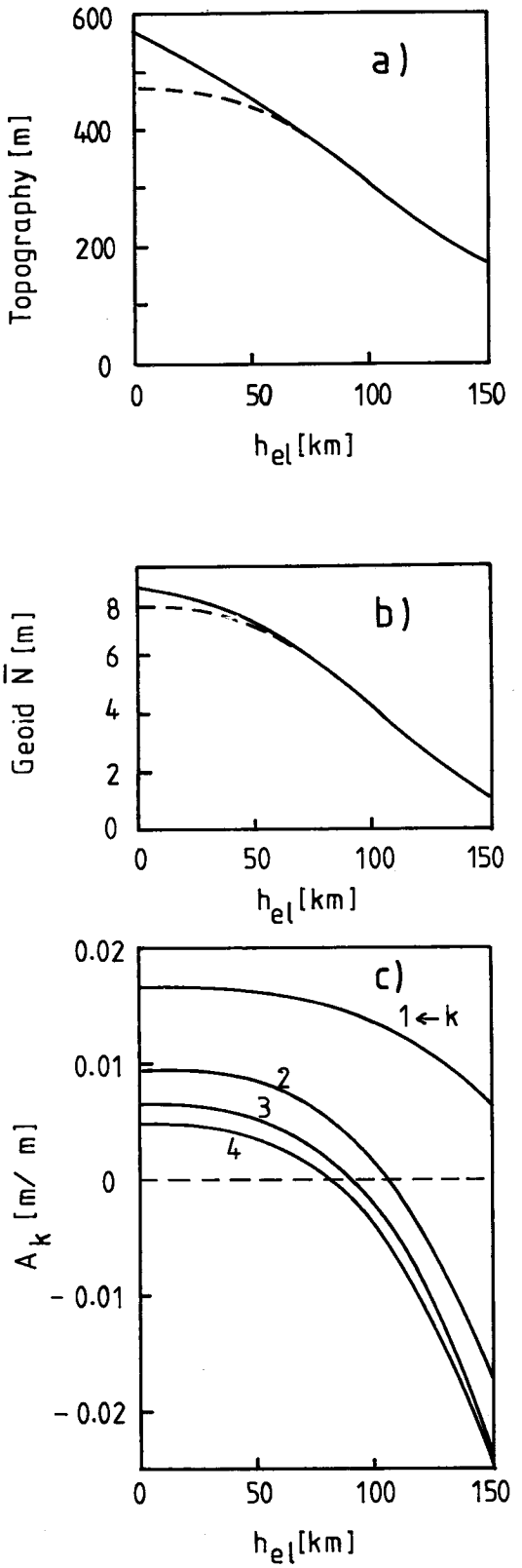

Figure 5. Peak to peak averaged amplitude for topography $\bar{w}$ and geoid undulation $\bar{N}$ and geoid admittance A as a function of the effective elastic thickness h_{el} for $a = 1$, $Ra = 10^5$ convection. The dashed lines in (a) and (b) indicate the values due to the basic coefficient in the Fourier expansion. In (c) admittance is given for the basic coefficient and for the next overtones.

overtones for $h_{el} > 70$ km; for the smallest aspect ratio (0.7) even the admittance of the fundamental wavelength (denoted by 1) becomes negative. The overtones are more strongly affected due to the mentioned low pass filtering of the elastic lithosphere. This is clearly demonstrated in Fig. 6, which shows the aspect ratio 1 spectra of geoid undulation and topography for $h_{el} = 0$ km (Fig. 6a and c) and $h_{el} = 150$ km (Fig. 6b and d). For $h_{el} = 0$ km the spectra contain a number of overtones while in case of $h_{el} = 150$ km only the longest wavelengths survived.

Figure 7 is a compilation of our results in case of $Ra = 10^5$. It shows surface topography $\bar{w}$, total geoid undulation $\bar{N}$ and free air gravity $\overline{\Delta g}$ depending on the elastic thickness of the lithosphere and the aspect ratio of the convection cell. Topography and geoid undulation increase strongly with increasing aspect ratio due to higher normal tractions transmitted to the lithospheric base. Yet the effect of a partly elastic lithosphere is, in absolute values, independent of the aspect ratio; increasing the elastic thickness from 0 to 150 km leads to a decrease in geoid undulation of the order of 10 m and in topography of about 450 m. However, the *relative* decrease of topography and geoid undulations with increasing h_{el} is much stronger for small aspect ratios than for large aspect ratios. For aspect ratios less than 1 the geoid might even become slightly negative above upwelling plumes. It should be noted here that taking the basic mode of the geoid undulation N_1 or topography w_1 rather than $\bar{N}$ or $\bar{w}$, shows that for large aspect ratios *no* decrease in N_1 or w_1 is obtained for increasing h_{el}, while for $a \approx 1$, N_1 and w_1 are still reduced strongly (see Fig. 12). This stems from the h_{el}^3 dependence of D in equation (13).

The effect of an elastic plate on free air gravity is even more pronounced (Fig. 7c). As gravity is related to geoid undulation by equation (25) shorter wavelengths are weighted more strongly. Therefore the thick elastic lithosphere as a low pass filter damps the relatively shorter wavelength overtones for small aspect ratios much more than overtones for higher aspect ratios.

Even though geoid and gravity admittances do not give direct information about the physical process involved, they are obtained by surface observables averaged over large areas and might therefore put constraints on the possible types of subcontinental convection. Geoid and gravity admittances for the fundamental wavelengths (denoted by index 1) depending on aspect ratio and h_{el} are given in Fig. 8(a and b) for $Ra = 10^5$.

Admittance values (Fig. 8a) are generally very high and are partly a consequence of the presence of an immobile lid which confines any convective temperature differences to depth greater than the lithospheric thickness h, thereby decreasing N_T and increasing the admittance. The elastic thickness of the lithosphere becomes important for $a < 1.5$ reducing the admittance down to even negative values. The gravity admittance of our models are given in Fig. 8(b). For small aspect ratio one can study the counteracting effects of the low pass filtering elastic lithospheric and of the amplification of smaller wavelength in the definition of the gravity.

For reasons of comparability the total lithospheric thickness was always 150 km, independent of h_{el}. This might be unrealistic in cases of a thin elastic part of the lithosphere. The effect of varying *both* the elastic and the

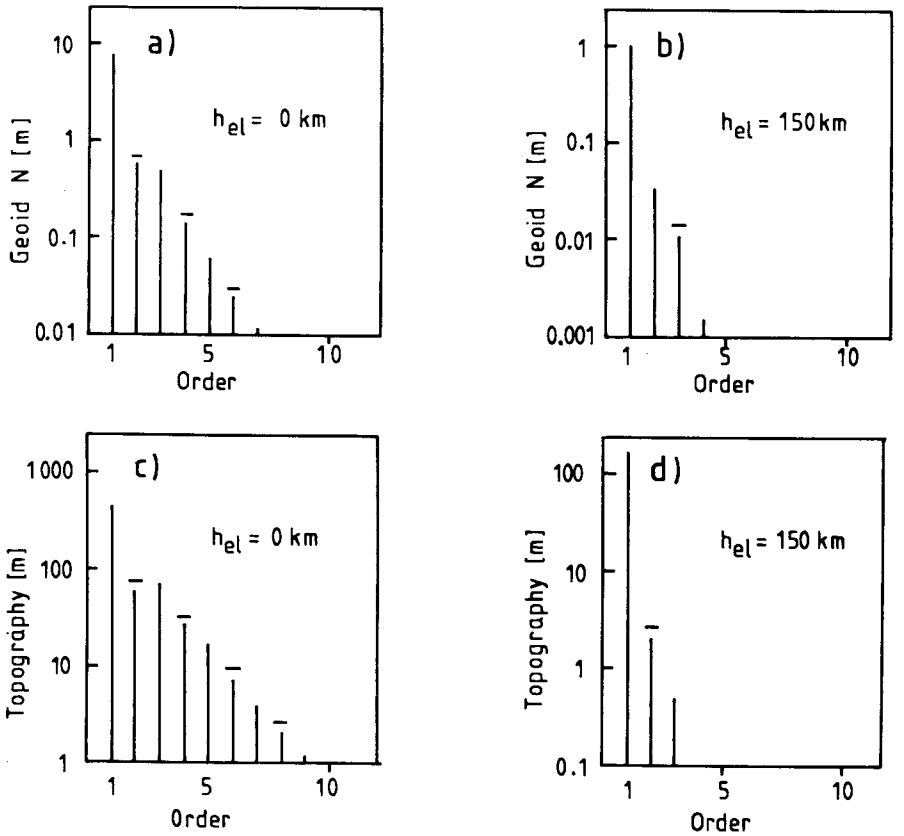

Figure 6. Spectra of geoid and topography for $a = 1$, $Ra = 10^5$ and (a, c) $h_{el} = 0$ km and (b, d) $h_{el} = 150$ km. The bars indicate coefficients with negative sign.

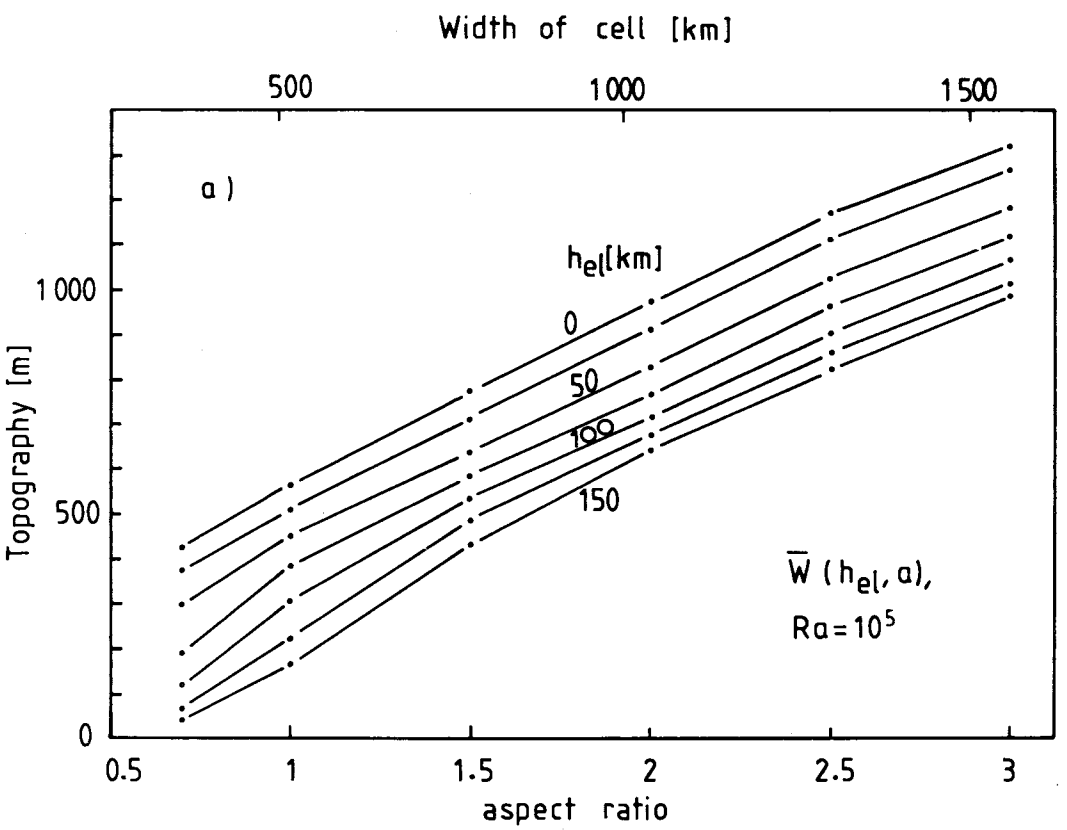

Figure 7. (a) Topography, (b) total geoid undulation and (c) free air gravity for $Ra = 10^5$, depending on aspect ratio of the convection and on the effective elastic thickness h_{el} of the lithospheric plate.

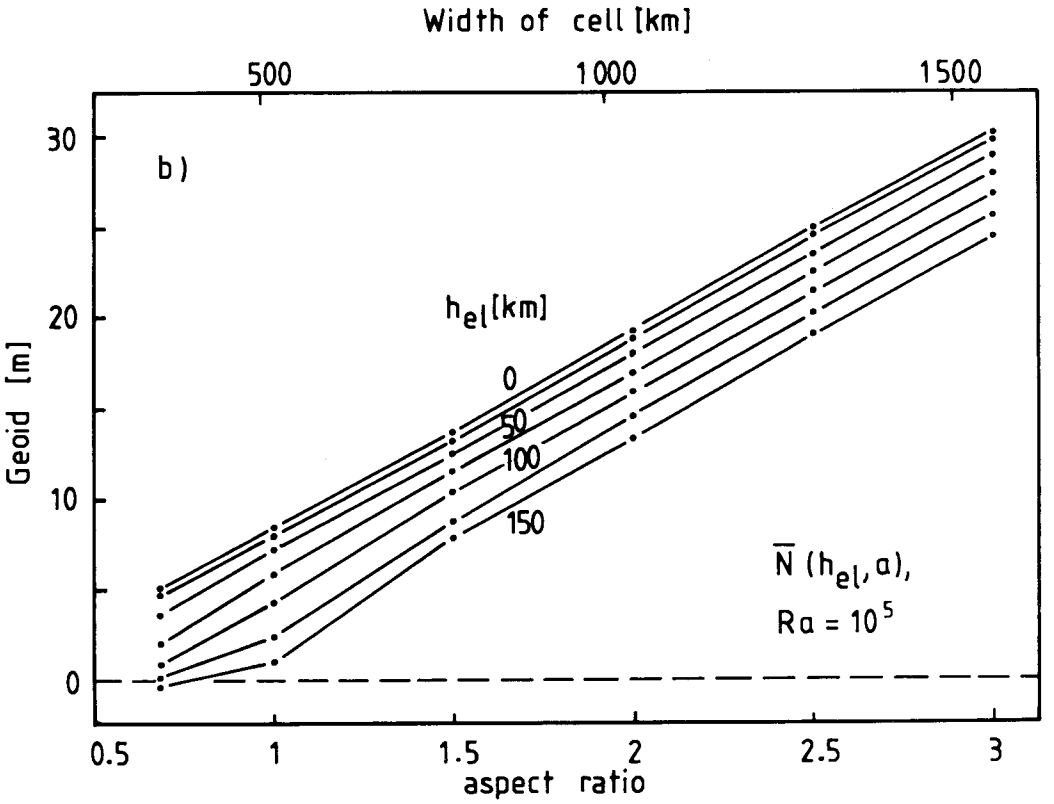

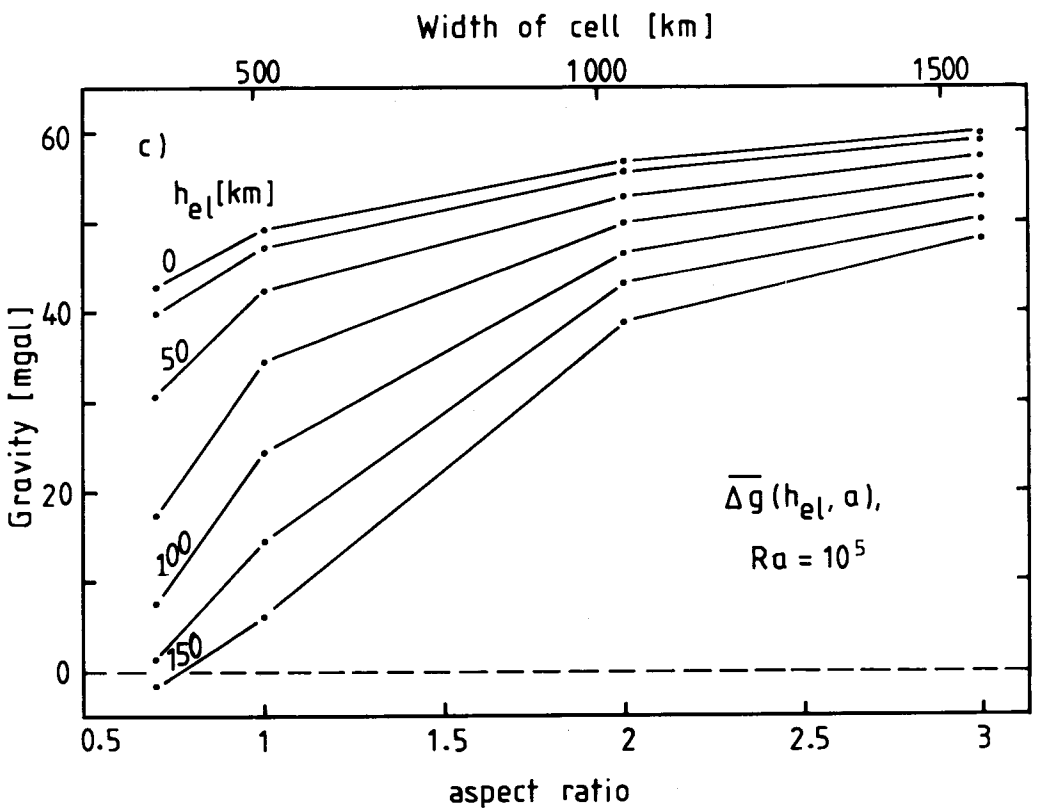

Figure 7. (*Continued*).

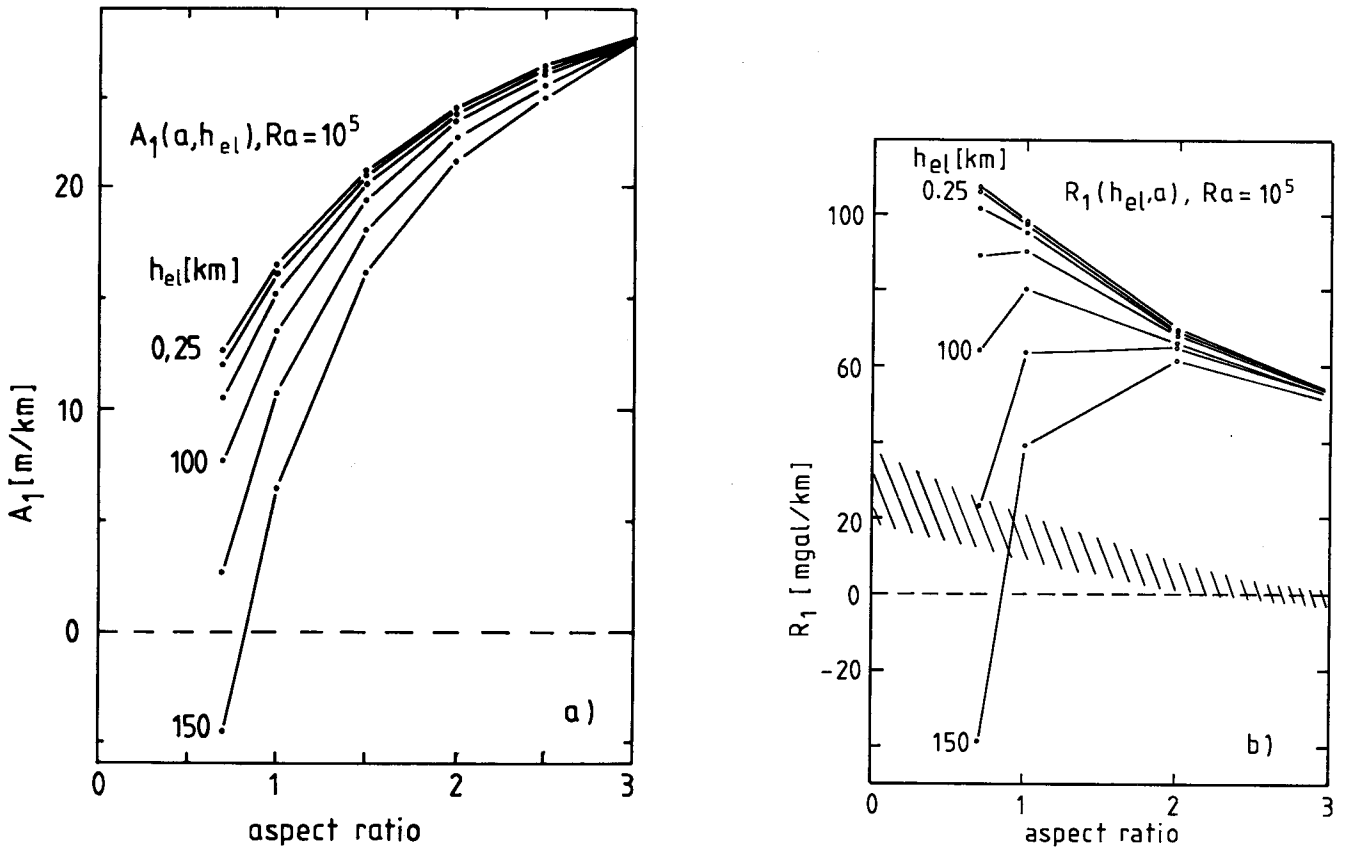

Figure 8. (a) Geoid admittance and (b) gravity admittance for the basic coefficients depending on the aspect ratio of the convection cell and the effective elastic thickness h_{el} of the lithosphere. Shaded area indicates observed free air gravity admittance values for North America (e.g. Lewis & Dorman 1970).

total thickness of the lithosphere (h_{el} and h) is shown in Fig. 9 in terms of lines of constant geoid undulation. For decreasing h, the geoid undulation decreases as well. This is because N_L remains constant, while N_{TP} increases due to the upper boundary coming closer to the surface. The previous results (Fig. 5b) can be found on the ordinate for $h = 150$ km. The lines of constant geoid undulation have a small slope for $h > 70$ km indicating that varying h between 70 and 150 causes only differences in geoid undulation of about 1 m or less. For $h < 70$ km differences can become greater, but these cases are not typical for stable continents.

In this section we will discuss the effects of variation in Rayleigh number. In this context it is important to carefully distinguish between *Ra* (scaling Rayleigh number of equation 6b) and Ra_q (Rayleigh number of constant heat flux, equation 7). If Ra_q is varied, an increase can be interpreted e.g. as lowering the viscosity or as increasing the heat input q, keeping the other quantities constant. In the first case, the boundary tractions will decrease leading to a *reduction* of geoid and topography, while in the second case additional heat input will accelerate the convection resulting in higher boundary tractions and thus *increase* in geoid and topography as it was found by Parsons & Daly (1983). In the first case *Ra* varies with Ra_q while in the second case *Ra* remains constant.

In our models we concentrate on the case of variations in

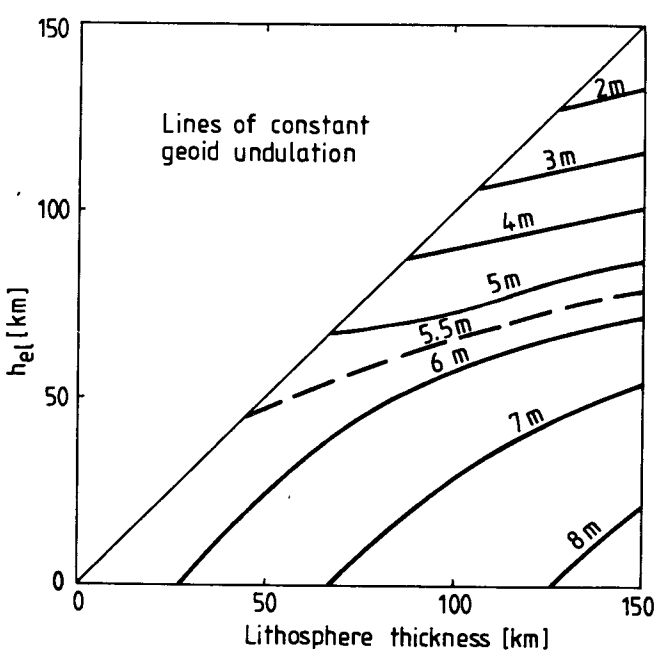

Figure 9. Lines of constant geoid undulation for $a = 1$ and $Ra = 10^5$ by varying the overall lithospheric thickness h and the effective elastic thickness h_{el}.

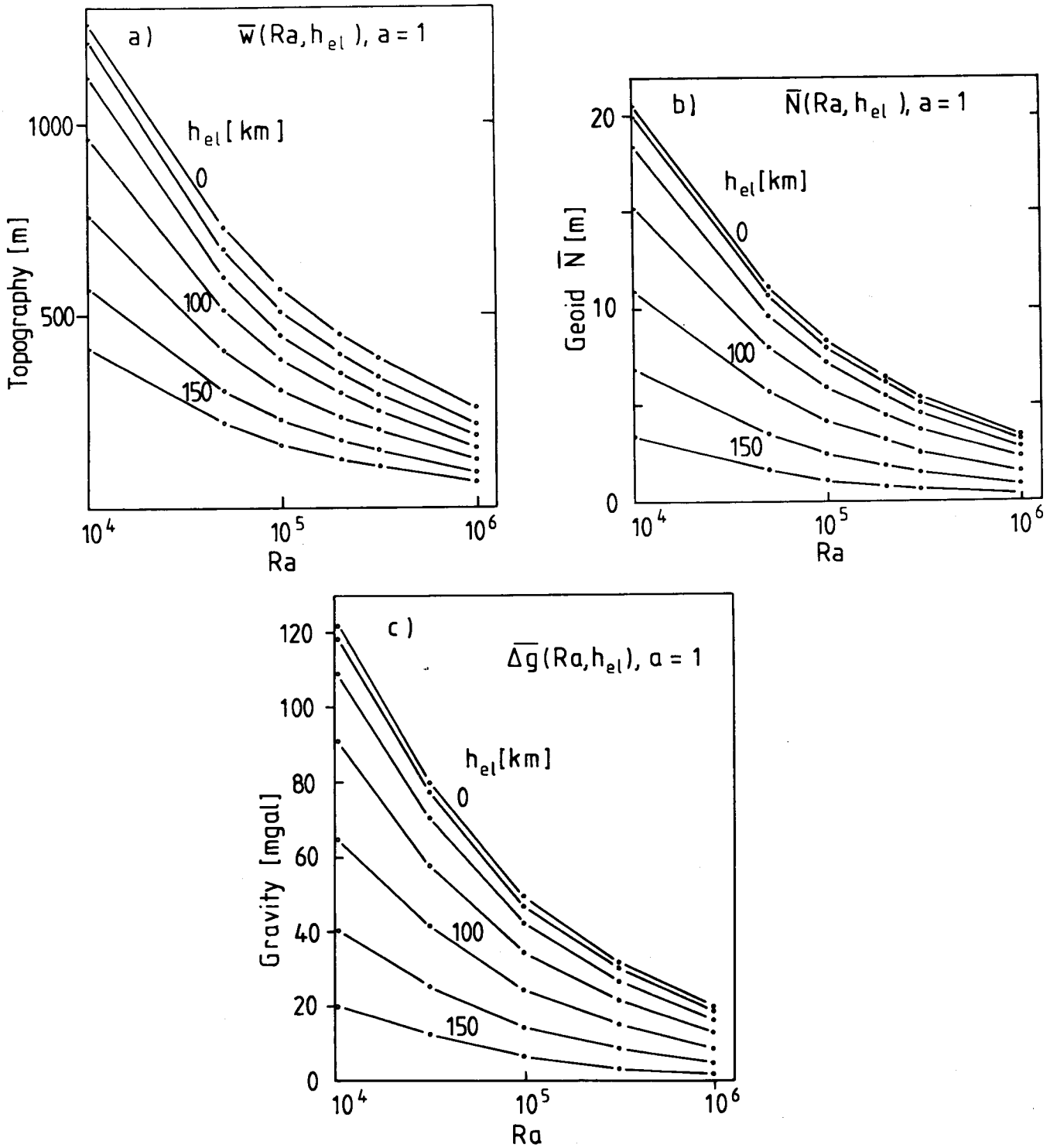

Figure 10. (a) Topography $\bar{w}$, (b) geoid undulation $\bar{N}$ and (c) free air gravity for $a = 1$, depending on the Rayleigh number of the convection and on the effective elastic thickness of the lithosphere.

viscosities and thus we varied Ra between 10^4 and 10^6. The results are plotted in Fig. 10(a–c) for topography, geoid undulation and gravity. The three curve-sets are similar, reflecting the dependence of the dimensional boundary tractions (σ_{z0}) from the Rayleigh number by

$$\sigma_{z0} = \frac{\kappa\eta}{d^2}\sigma'_{z0} \sim \frac{\kappa\eta}{d^2} Ra_q^{\gamma} \sim \eta^{1-\gamma},$$

where σ'_{z0} are the non-dimensional tractions. γ is found to be approximately 0.5 (e.g. McKenzie 1977; Parsons & Daly 1983).

For low Rayleigh number very high values for topography, geoid undulations and gravity are found. For $Ra = 10^4$ topography reaches values of about 2000 m for peak to peak amplitude. Such values are only observed in mountain ranges, but normally associated with much lower

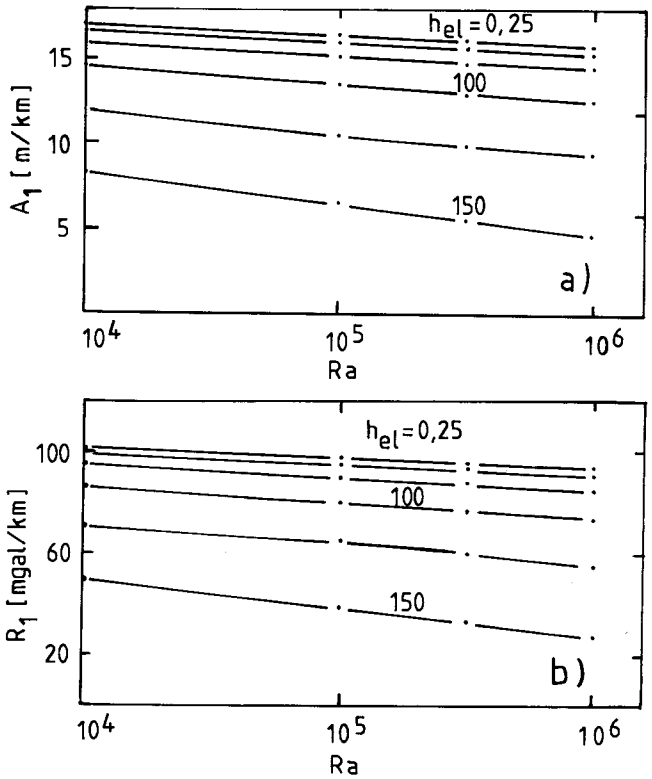

Figure 11. (a) Geoid and (b) gravity admittance of the basic coefficient for aspect ratio 1 depending on h_{el} and the Rayleigh number.

geoid and free air gravity values, indicating a thickening of the lithosphere due to isostasy or down-welling flow in collision belts.

Even though the surface observables very strongly depend on *Ra*, the geoid and gravity admittances for the basic coefficient only slightly decrease, approximately linearly, with increasing *Ra* (Fig. 11).

5 DISCUSSION

Before comparing our results with observations it has to be noted that most of the previous investigations have calculated the geoid directly on top of the convective system; that means they did not consider an overlying plate. This approach is appropriate if the plate represents a dynamic part of the convective cell, as it is the case of spreading oceanic plates. However, for sublithospheric convection beneath continents two effects lead to important differences between our models including a plate and previous models. (i) Elasticity of the plate reduces the topography and thus N_L and the admittance; and (ii) all convective temperature differences are confined to a depth below the lithosphere, this leads to decreasing N_T and increasing admittance. In fact, inspection of equation (21) shows that N_{TP} at the earth's surface is reduced by a factor of $\exp(-nkh)$ compared to the geoid undulations at a level immediately above the convective cell. As a consequence of (ii) the geoid admittance of the basic coefficients of our models, which are shown in Fig. 8(a), are relatively high.

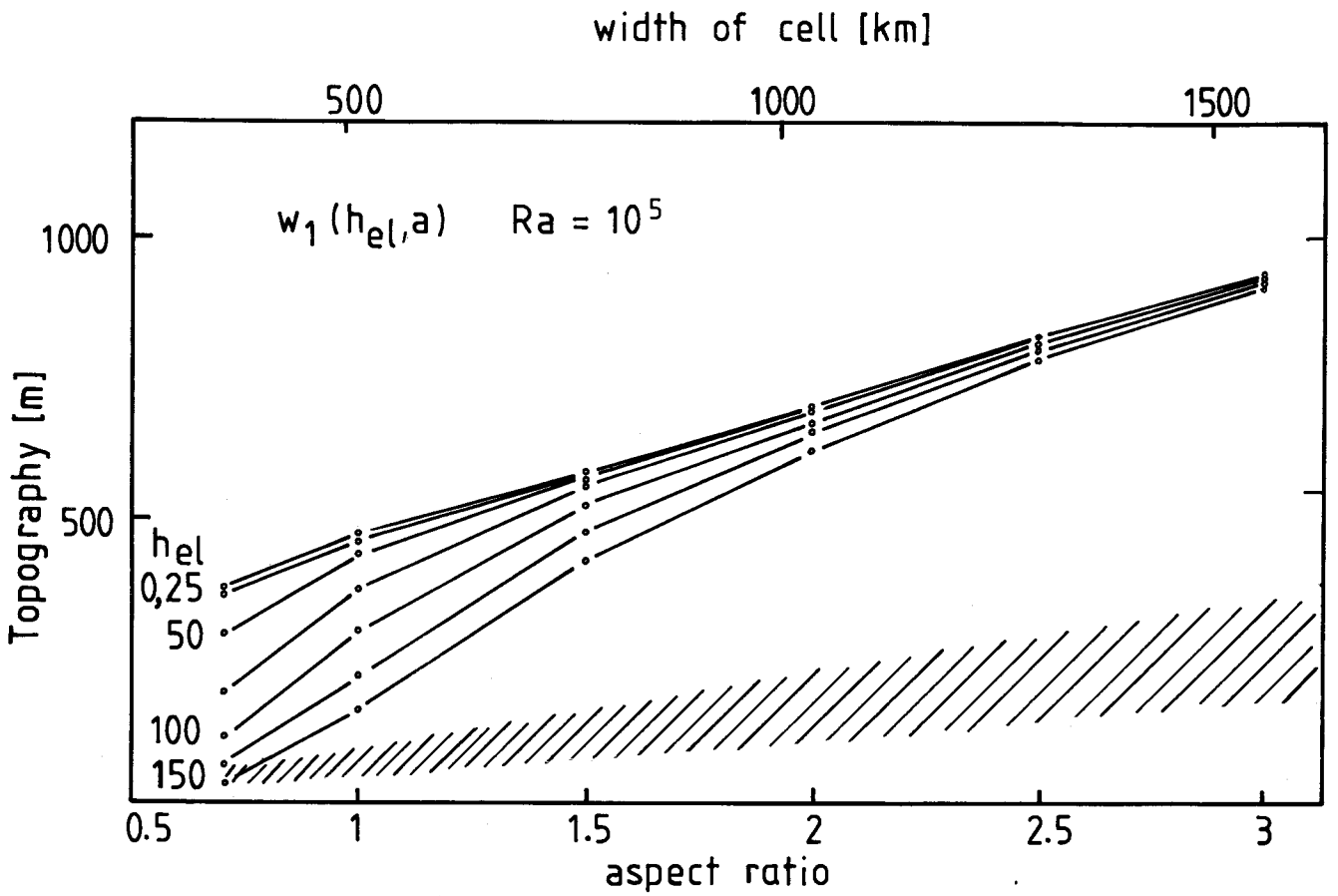

Figure 12. Basic coefficient topography w_1 for $Ra = 10^5$ depending on aspect ratio and h_{el}. Observed topography for North America for the wavelengths considered lie in the dashed area (e.g. Lewis & Dorman 1970).

Parsons & Daly (1983) obtained only values around 5–6 m km^{-1} for $Ra = 10^5$ and an aspect ratio of 1 by inspecting the geoid to topography relation in space domain.

It should be noted, however, that our models neglect any lateral temperature variations within the plate. To assess this effect, we consider a plate showing long wavelength variation in mean tempeature of the order δT which would lead to corresponding variations in thickness of the order $\delta h \simeq h\alpha\,\delta T$. Regarding this δh being compensated by a Pratt-like isostasy with compensation depth h_c, the corresponding geoid undulation is (Turcotte & Schubert 1982)

$$N = \frac{\pi G}{g}\rho_s h_c w = \frac{\pi G}{g}\rho_s h_c^2 \alpha\,\delta T. \tag{27}$$

For our models, lateral variations of temperature in the lithosphere of 50 °K would lead to additional topography of about 220 m and geoid undulation of about 3 m. However, we believe that such temperature variations are small compared to those occurring in the convective flow itself (*cf.* Fleitout & Yuen 1984, who modelled a highly viscous plate on top of a convective flow).

To relate our models to nature and to put constraints on possible aspect ratios, lithospheric thickness and Rayleigh number we refer to the well-known paper by Lewis & Dorman (1970). They studied surface observables in spectral domain for North America which can be regarded as upper bounds of our models. They found amplitude values for topography below 1000 m for the longest wavelength studied. For wavelenths corresponding to our asepect ratios of 0.7–3 the topography data range between 20 and 400 m (see dashed area in Fig. 12). This suggests that only models with a thick elastic plate (>110 km), a small aspect ratio (<1) and a high Rayleigh number (>10^5) may be compatible with the data (see Figs 10a and 12). For the gravity admittance, Lewis & Dorman (1970) found values ranging from 0 to 40 mGal m^{-1} (dashed area in Fig. 8b), depending on the wavelengths. Very long wavelength topography seems to be compensated by crustal and/or lithospheric thickening leading to vanishing free air gravity and thus R_1 cannot be related to any convective flow. For short wavelength loading ($a \leq 1$) and a thick elastic lithosphere, low R_1 values are predicted by our models and fall below the observed bounds. Fig. 10(c) suggests that observed gravity data of about 20 mgal for wavelengths associated with aspect ratio 1 indicate a preference of high Rayleigh numbers (>10^5) for possible small-scale subcontinental convection.

At this point we should note that we do not necessarily interpret the observed data as a result of convective flow since sources within the lithosphere are possible as well. We only emphasize that the data do not permit convection for certain parameter ranges discussed above. Only in connection with other data like those discussed in the introduction can our results be used to infer subcontinental convection.

Often long wavelength geoid undulations and topography are interpreted in terms of Pratt compensating mass distributions (Haxby & Turcotte 1978) using equation (27) to estimate the depth of compensation from N and w. However, Parsons & Daly (1983) and, recently, Robinson, Parsons & Daly (1987) have argued that in case of dynamically produced topography and geoid undulations as in the case of convection, estimates of h_c assuming Pratt compensation may be misleading, especially for variable viscosity distributions. In particular, Robinson *et al.* (1987) calculated geoid undulations and topography for upper mantle convection beneath a highly viscous oceanic plate assuming a low viscosity asthenosphere and found that the apparent h_c drastically decreases for decreasing asthenospheric viscosity. From our calculations we can use the longest wavelength components of N and w to obtain the ratio $A_1 = N_1/w_1$ and estimate apparent depths of compensation h_c from (27). For the highest A_1 values in Fig. 8(a) (i.e. for large aspect ratio cells) we obtain $h_c = 400$ km, which lies well within the convecting layer (although not at its base at 670 km depth). However, for aspect ratio 1 cells and elastic lithospheric thicknesses greater or around 100 km, h_c becomes less than 150 km. Note, that in our models the driving density contrasts are *below* 150 km depth. We thus conclude that in continental regions assumptions on Pratt compensation mass distributions may underestimate the depth of compensation.

6 CONCLUSION

In this study we have investigated the effect of small-scale sublithospheric convection on topography, geoid and their spectral relation. We modelled the lithosphere as a partly elastic plate mechanically coupled to the viscous mantle. One of our aims was to show that, at least for continental regions, very low (and even negative) admittance values might occur even in the case of a constant viscosity mantle. Due to the low pass filter behaviour of an elastic plate this effect will increase with decreasing wavelength depending on the λ/h_{el} relation. Therefore the higher harmonics are always affected more strongly than the basic mode. In case of aspect ratio 0.7, which is related to a horizontal dimension of the convection cell of 364 km, an elastic thickness of 150 km will give rise to a negative admittance even for the basic mode, which means negative geoid undulation above the upwelling plume. On the other hand, it also turned out (Fig. 5) that an elastic thickness less than 50 km will have negligible influence showing that for oceanic or thinned continental areas such as rift valleys the effect of the elastic strength of the lithosphere is not important. For old continental shields and platforms, however, it might lead to a significant lowering of topography, geoid, and their related admittance.

A brief comparison with the observed gravity transfer function for the North American continent shows that large aspect ratio cells beneath continents are unlikely. However, aspect ratio 1 cells beneath plates of at least 100 km effective elastic thickness are in agreement with the data. Additional observables such as surface heat flux or lithospheric thickness variations also show strong possibility for convection below stable continents. A systematic regional correlation between assessable observables, as well as more realistic models with e.g. variable viscosity, would be the next step to actually prove the existence of sublithospheric convection below continents.

ACKNOWLEDGMENTS

We are grateful for stimulating discussions with Ulrich Christensen and Luce Fleitout. An anonymous reviewer provided helpful comments on the manuscript. This study was supported by the grant G-GU 3114-127 of the Swedish Natural Research Council (NFR).

REFERENCES

Babuska, V., Plomerova, J. & Sileny, J., 1987. Structural model of the subcrustal lithosphere in central Europe, in *Composition, structure and dynamics of the lithosphere–asthenosphere system*, AGU Geodynamics Series No 16, pp. 239–251, eds Fuchs, K. & Froidevaux, C., AGU.

Byerlee, J. D., 1978. Friction of rocks, *Pageoph*, **116**, 613–626.

Cazenave, A., Dominh, K., Allegre, C. J. & Marsh, J. G., 1986. Global relationship between oceanic geoid and topography, *J. geophys. Res.*, **91**, 11439–11450.

Cazenave, A. & Dominh, K., 1987. Global relationship between oceanic geoid and seafloor depth: new results, *Geophys. Res. Lett.*, **14**, 1–4.

Christensen, U. R., 1983. A numerical model of coupled subcontinental and oceanic convection, *Tectonophys.*, **95**, 1–23.

Christensen, U. R., 1987. Time-dependent convection in elongated Rayleigh–Benard cells, *Geophys. Res. Lett.*, **14**, 220–223.

Cserepes, L. & Rabinowicz, M., 1985. Gravity and convection in a two layered mantle, *Earth planet. Sci. Lett.*, **76**, 193–207.

Davies, G. F., 1986. Mantle convection under simulated plates, effects of heating modes and ridge and trench migration, and implications for the core-mantle boundary, bathymetry, the geoid and Benioff zones, *Geophys. J. R. astr. Soc.*, **84**, 153–183.

Davies, G. F. & Strebeck, J. W., 1982. Old continental geotherms: Constraints on heat production and thickness of continental plates, *Geophys. J. R. astr. Soc.*, **69**, 623–634.

Fleitout, L. & Yuen, D., 1984. Steady state, secondary convection beneath lithospheric plates with temperature- and pressure-dependent viscosity, *J. geophys. Res.*, **89**, 9227–9244.

Forsyth, D. W., 1985. Subsurface loading and estimates of the flexural rigidity of continental lithosphere, *J. geophys. Res.*, **90**, 12623–12632.

Goetze, G., 1978. The mechanism of creep in olivine, *Phil. Trans. R. Soc.* **A288**, 99–119.

Goetze, G. & Evans, B., 1979. Stress and temperature in the bending lithosphere as constrained by experimental rock mechanism, *Geophys. J. R. astr. Soc.*, **59**, 463–478.

Gurnis, M., 1988. Large-scale mantle convection and the aggregation and dispersal of supercontinents, *Nature*, **332**, 695–699.

Hager, B. H., 1984. Subducted slabs and the geoid: Constraints on mantle rheology and flow, *J. geophys. Res.*, **89**, 6003–6015.

Haxby, W. F. & Turcotte, D. L., 1978. On isostatic geoid anomalies. *J. geophys. Res.*, **83**, 5473–5478.

Haxby, W. F. & Weissel, J. K., 1986. Evidence for small-scale mantle convection from *SEASAT* altimeter data, *J. geophys. Res.*, **91**, 3507–3520.

Jarvis, G. T. & McKenzie, D. P., 1980. Convection in a compressible fluid with infinite Prandtl number, *J. Fluid Mech.*, **96**, 515–583.

Karner, G. D. & Watts, A. B., 1983. Gravity anomalies and flexure of the lithosphere at mountain ranges, *J. geophys. Res.*, **88**, 10449–10477.

Kirby, S. H., 1983. Rheology of the lithosphere, *Rev. Geophys. Space Phys.*, **21**, 1458–1487.

Koch, M. & Yuen, D. A., 1985. Surface deformations and geoid anomalies over single and double layered convective systems, *Geophys. Res. Lett.*, **12**, 701–704.

Kogan, M. G. & McNutt, M. K., 1987. Isostasy in the USSR I: Admittance data, in *Composition, Structure and Dynamics of the Lithosphere–asthenosphere System*, AGU Geodynamics Series, 16, pp. 301–307, eds Fuchs, K. & Froidevaux, C., AGU.

Lewis, B. T. R. & Dorman, L. M., 1970. Experimental isostasy: 2. An isostatic model for the U.S.A. derived from gravity and topography data, *J. geophys. Res.*, **7**, 3367–3386.

Marquart, G., 1987. On modelling the deflection of an elastic lithosphere: thin plate approximation versus numerical modelling, *Report No. 30*, Institute of Geophys, Uppsala University.

McKenzie, D. P., 1977. Surface deformation, gravity anomalies and convection, *Geophys. J. R. astr. Soc.*, **48**, 211–238.

McKenzie, D. P., Roberts, J. M. & Weiss, N. D., 1974. Convection in the earth's mantle: towards a numerical solution, *J. Fluid Mech.*, **62**, 465–538.

McKenzie, D. P. & Bowin, C., 1976. The relationship between bathymetry and gravity in the Atlantic Ocean, *J. geophys. Res.*, **81**, 1903–1915.

McKenzie, D. P., Watts, A., Parsons, B. & Roufosse, M., 1980. Planform of mantle convection beneath the Pacific Ocean, *Nature*, **288**, 442–446.

Molnar, P. & Tapponnier, P., 1981. A possible dependence of tectonic strength on the age of the crust in Asia, *Earth planet. Sci. Lett.*, **52**, 107–114.

Parsons, B. & Daly, S., 1983. The relationship between surface topography, gravity anomalies, and temperature structure of convection, *J. geophys. Res.*, **88**, 1129–1144.

Peltier, W. R. & Wu, P., 1983. Continental lithospheric thickness and deglaciation induced true polar wander, *Geophys. Res. Lett.*, **10**, 181–184.

Pollack, H. N. & Chapman, D. S., 1977. On the regional variation of heat flow, geotherms and lithospheric thickness, *Techonophys.*, **38**, 279–296.

Pujol, J., Fountain, D. M. & Anderson, D. A., 1985. Statistical analysis of the mean heat flow/reduced heat flow relationship for continents and its tectonothermal implications, *J. geophys. Res.*, **90**, 11335–11344.

Ricard, Y., Fleitout, L. & Froidevaux, C., 1984. Geoid heights and lithospheric stresses for a dynamic earth, *Ann. Geophys.*, **2**, 267–286.

Richards, M. A. & Hager, B. H., 1984. Geoid anomalies in a dynamic earth, *J. geophys. Res.*, **89**, 5987–6002.

Richter, F. H., 1973. Convection and the large-scale circulation of the mantle, *J. geophys. Res.*, **78**, 8734–8745.

Richter, F. M. & Parsons, B., 1975. On the interaction of two scales of convection in the mantle, *J. geophys. Res.*, **80**, 2529–2541.

Robinson, E. M., Parsons, B. & Daly, S. F., 1987. The effect of a shallow low viscosity zone on the apparent compensation of mid-plate swells, *Earth planet. Sci. Lett.*, **82**, 335–348.

Schmeling, H., 1980. *Numerische Konvektionsrechnungen unter Annahme verschiedener Viskositaetsverteilungen und Rheologien im Mantel.* Bericht des Inst. für Meteorologie u. Geophysik der Univ. Frankfurt/M.

Schmeling, H. & Jacoby, W. R., 1981. On modelling the lithosphere in mantle convection, *J. Geophys.*, **50**, 89–100.

Schmeling, H., 1987. On the interaction between small- and large-scale convection and postglacial rebound flow in a power-law mantle, *Earth planet. Sci. Lett.*, **84**, 254–262.

Sclater, J. G., Jaupart, C. & Galson, D., 1980. The heat flux through oceanic and continental crust and the heat loss of the earth, *Rev. Geophys. Space Phys.*, **18**, 269–311.

Souriau, M. & Souriau, A., 1983. Test of tectonic models by great circle Rayleigh waves, *J. geophys. Res.*, **88**, 2273–2288.

Stocker, R. L. & Ashby, M. F., 1973. On the rheology of the upper mantle, *Rev. Geophys. Space Phys.*, **11**, 391–426.

Turcotte, D. L. & Schubert, G., 1982. *Geodynamics*, J. Wiley, New York.

Vitorello, I. & Pollack, H. N., 1980. On the variation of continental heat flow with age and the thermal evolution of the continents, *J. Geophys.*, **85**, 983–995.

Walcott, R. I., 1970. Flexural rigidity, thickness and viscosity of the lithosphere, *J. geophys. Res.*, **75**, 3941–3954.

Watts, A. B., Bodini, J. H. & Ribe, N. M., 1980. Observations of flexure and the geophysical evolution of the Pacific basin, *Nature*, **283**, 532–537.

Watts, A. B. & Daly, S. F., 1981. Long wavelength gravity and topography anomalies, *Ann. Rev. Earth planet. Sci.*, **9**, 415–448.

Watts, A. B. & Ribe, N. M., 1984. On geoid height and flexure of the lithosphere at seamounts, *J. geophys. Res.*, **89,** 11152–11171.

Weertman, J., 1970. The creep strength of the earth's mantle, *Rev. Geophys. Space Phys.*, **8,** 145–168.

Wolf, D., 1987. An upper bound on lithospheric thickness from glacio-isostatic adjustment in Fennoscandia, *J. Geophys.*, **61,** 141–149.

Yuen, D. A., Sabadini, R. & Boschi, E., 1983. The dynamic equations of polar wander and the global characteristics of the lithosphere as extracted from rotational data, *Phys. Earth planet. Int.*, **33,** 226–242.